

Direct characterization of ultrafast energy-time entangled photon pairs

Jean-Philippe W. MacLean,^{1,2,*} John M. Donohue,^{1,2,3} and Kevin J. Resch^{1,2}

¹*Institute for Quantum Computing, University of Waterloo, Waterloo, Ontario, Canada, N2L 3G1*

²*Department of Physics & Astronomy, University of Waterloo, Waterloo, Ontario, Canada, N2L 3G1*

³*Integrated Quantum Optics, Applied Physics, University of Paderborn, 33098 Paderborn, Germany*

(Dated: November 1, 2017)

Energy-time entangled photons are critical in many quantum optical phenomena and have emerged as important elements in quantum information protocols. Entanglement in this degree of freedom often manifests itself on ultrafast timescales making it very difficult to detect, whether one employs direct or interferometric techniques, as photon-counting detectors have insufficient time resolution. Here, we implement ultrafast photon counters based on nonlinear interactions and strong femtosecond laser pulses to probe energy-time entanglement in this important regime. Using this technique and single-photon spectrometers, we characterize all the spectral and temporal correlations of two entangled photons with femtosecond resolution. This enables the witnessing of energy-time entanglement using uncertainty relations and the direct observation of nonlocal dispersion cancellation on ultrafast timescales. These techniques are essential to understand and control the energy-time degree of freedom of light for ultrafast quantum optics.

The energy-time degree of freedom of non-classical light is of great interest for quantum information as it supports various encodings, including frequency bins [1], time bins [2], and broadband temporal modes [3], and is intrinsically robust for propagation through long-distance fibre links [4]. Applications which harness quantum correlations in this degree of freedom, referred to as energy-time entanglement [5], include dispersion cancellation [6, 7], high-dimensional quantum key distribution [8, 9], and quantum-enhanced clock synchronization [10]. In ultrafast optics and attosecond physics, the ability to measure both frequency and temporal features has led to important innovations in electric field reconstruction techniques [11, 12] and pulse characterization on very short timescales, enabling advances in spectroscopy [13], laser physics [14], nonlinear optics [15], and imaging [16]. In order to characterize and control energy-time entangled photons and advance biphoton pulse shaping, similar measurement capabilities are essential in the quantum regime.

Experimental signatures of entanglement can arise in correlation measurements of complementary variables [17], or through nonlocal quantum effects [5, 6]. With the energy-time degree of freedom, one complementary set consists of measuring the intensity correlations as a function of the photon frequencies and as a function of their time of arrival. These have been individually realized for different photonic systems with measurements in frequency [18, 19] or in time [20–22]. Certifying the presence of entanglement with direct measurements requires both spectral and temporal correlations, since acquiring only one remains insufficient to uniquely specify the other due to the ambiguity of the spectral phase. Depending on the platform, this can be challenging. Narrow-band photons from atomic systems can be readily mea-

sured in time but are difficult to spectrally resolve [22]. THz-bandwidth photons produced in spontaneous parametric downconversion (SPDC) are often characterized spectrally, but they can have features on femtosecond timescales below current detector resolution [23].

Other techniques can be employed to infer the presence of energy-time entanglement. High-order interference effects with Franson interferometers have been used to illustrate entanglement between two [24] and three photons [25]. Nonlocal dispersion cancellation [6], whereby the temporal spread in coincidences remains unchanged when equal and opposite dispersion is applied to each photon, can also be used to witness entanglement [26, 27]. For either method to be effective, the detector resolution must be shorter than the timescales of the correlations. Strong energy-time entanglement can nonetheless exist when the timescales of the correlations are shorter. Certain observations have pointed to nonlocal dispersion cancellation in this regime, but they either required introducing a very large amount of dispersion such that temporal resolution could be achieved with standard detectors [28], or used sum-frequency generation (SFG) between the photons pairs [29], which, unlike measurements with fast and independent detectors, has a close classical analogue [30]. Directly measuring ultrafast quantum effects requires new methods to control and analyze single photons in the time domain.

In nonlinear optics and laser physics, optical gating is widely used to overcome limitations with detectors which are too slow to observe features on subpicosecond timescales. The gating is achieved by combining the signal with a short gate pulse in a nonlinear medium and measuring the upconversion signal on the detector. With fast gates and slow detectors, an effective fast de-

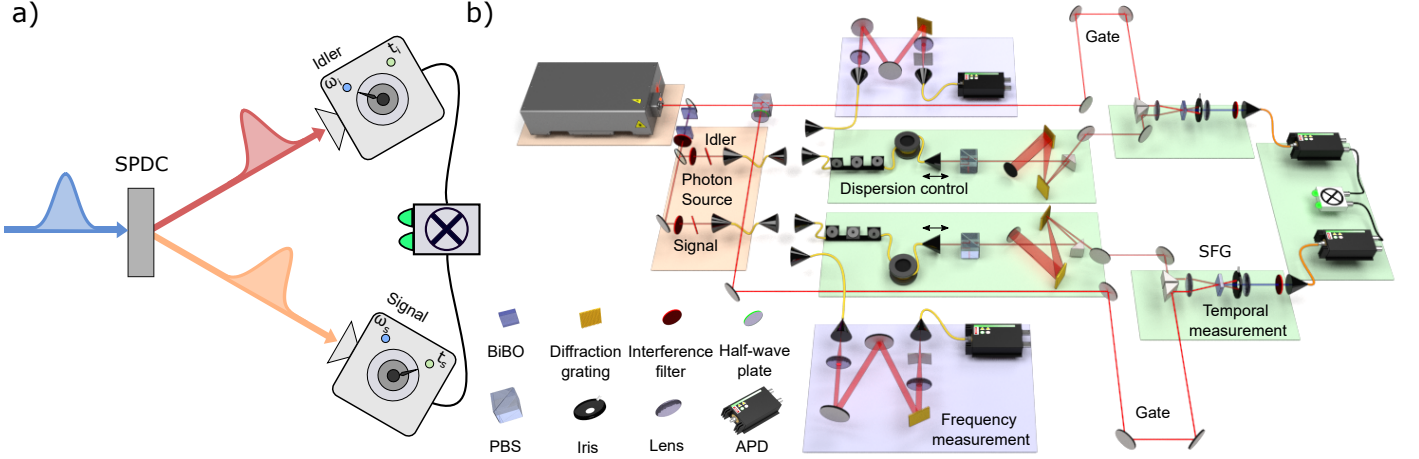


FIG. 1. **Experimental setup.** (a) Frequency-entangled photons are created through spontaneous parametric downconversion of an ultrafast pulse from a frequency doubled Ti:sapphire laser. Measurements of either the frequency or the time of arrival of each photon can be performed in coincidence. (b) Spectral measurements are made with dual single-photon monochromators. Temporal measurements are performed using optically gated single-photon detection. The gating is implemented via noncollinear sum-frequency generation between a strong gate pulse from the Ti:Sapph laser and the signal or idler. The dispersion of the signal and idler photons is controlled with a combination of single mode fibres and grating compressors before the upconversion. The upconverted signal is filtered with bandpass filters which remove the background second harmonic generation from the gate pulse. Temporal and frequency measurements are performed in coincidence to observe the spectral and temporal features of the photons.

tector can be engineered to temporally resolve single photons [31, 32] and photon pairs [20]. In this work, we develop fast optical gating to achieve subpicosecond timing resolution for spatially separated pairs of single photons. We use this technique in conjunction with single-photon spectrometers to explicitly measure both the spectral and temporal correlations of broadband photons, as well as the cross-correlations between the frequency of one photon and time of arrival of the other. Furthermore, by controlling the dispersion of each photon, our high-resolution joint temporal measurements make it possible to directly observe nonlocal dispersion cancellation on femtosecond timescales.

Through spectral and temporal measurements, energy-time entanglement can be witnessed by violating uncertainty relations [33, 34]. Two separable photons or classical pulses must satisfy the following inequality [17, 21],

$$\Delta(\omega_s + \omega_i)\Delta(t_s - t_i) \geq 1, \quad (1)$$

where each photon, labelled signal and idler, is described by its frequency ω and its time of arrival t , and Δ represents the standard deviation in the joint spectrum or joint temporal intensity. In other words, there is a non-trivial limit to the strength of the product of correlations between the sum of the frequencies and the difference in time of arrival if the photons are separable. However, this is not the case for energy-time entangled photons where the right side of Eq. 1 can approach zero. Thus, the uncertainty relation is an entanglement witness.

Two-photon states produced via SPDC are often energy-time entangled. In downconversion, energy con-

servation tends to lead to entangled states with frequency anti-correlations, although engineering SPDC sources have been explored to produce photon pairs with uncorrelated [35] or even positively correlated frequencies [36–40]. For a pure state with no spectral phase, strong frequency correlations imply strong correlations in the time of arrival of the photons. Under these conditions, Eq. 1 can be violated provided one has sufficient resolution in the measurements.

Our experimental setup is shown in Fig. 1. The laser output at 775 nm is frequency doubled to 387.5 nm in 2 mm of bismuth-borate (BiBO). The resulting pump light is spectrally narrowed using a 0.085 nm ($1/\sqrt{e}$) bandpass filter. Signal and idler photon pairs are created through type-I SPDC of the pump in 5 mm of BiBO with central wavelengths of 729 nm and 827 nm, respectively. The bandwidths are controlled using tunable spectral edge filters after which the photons are coupled to single-mode fibres. The fibres allow for easy switching between spectral measurement, temporal measurement, and direct detection. The dispersion of the fibre links is then compensated with grating-based pulse compressors. Spectral measurements are performed with grating-based scanning monochromators with a resolution of about 0.1 nm. Temporal measurements are performed through sum-frequency generation in 1 mm of type-I BiBO with a strong gate laser pulse with an intensity temporal width of 120 fs ($1/\sqrt{e}$), measured using an auto-correlation and assuming a Gaussian spectrum. The upconverted photons are detected after passing through spectral bandpass filters which remove the second harmonic background of the gate pulse. We estimate the absolute efficiency of

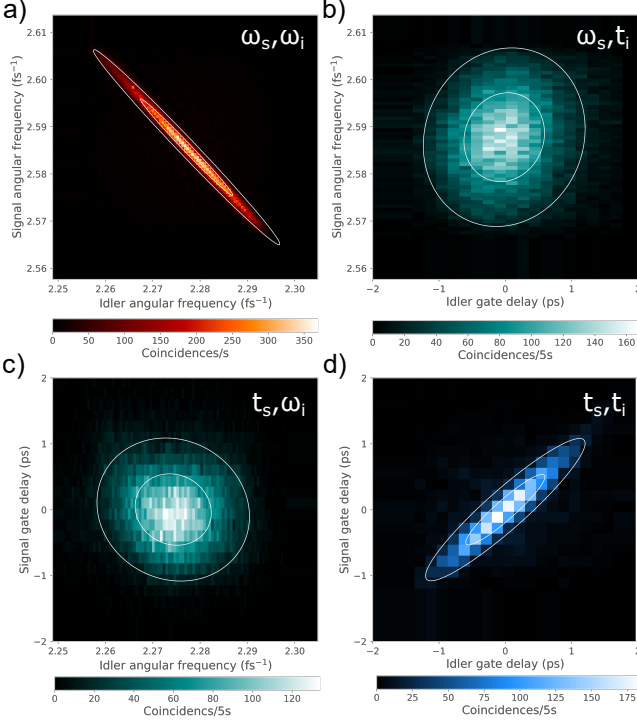


FIG. 2. **Spectral and temporal characterization of ultrafast photons.** A combination of spectral and temporal measurements are made in coincidence in order to measure (a) the joint spectrum, (d) the joint temporal intensity, as well as the (b,c) cross-correlations between the time (frequency) of the idler and frequency (time) of the signal. (a) Frequency anti-correlations with statistical correlation -0.9951 ± 0.0001 , are accompanied with (d) positive correlations 0.987 ± 0.004 in the signal-idler arrival times. The time-frequency plots (c,d) show little correlations, (-0.106 ± 0.007) and (0.110 ± 0.007) , respectively, indicating low dispersion in the signal and idler photons. White lines on all plots correspond to 1σ and 2σ contours of two-dimensional Gaussian fits.

the temporal apparatus, including fibre coupling, chirp compensation, and upconversion, to be 3% of the maximum possible. Detection events for the signal and idler are measured in coincidence after they have passed either through both spectrometers, both temporal gates, or one of each. The corresponding measured joint spectrum, joint temporal intensity, and time-frequency plots, which measure the frequency of one photon in coincidence with the arrival time of the other, are shown in Fig. 2. Background subtraction has not been employed in the data.

For each joint measurement of Fig. 2, the marginal width is obtained by fitting the marginals to a one-dimensional Gaussian, while the heralded width is obtained taking the average of several slices of the data when the frequency or time of one photon is fixed. The statistical correlation, ρ , is obtained by finding the value that best fits a two-dimensional Gaussian with the measured marginals. Since the finite resolution of both spec-

TABLE I. **Ultrafast two-photon state parameters.** Measured marginals, heralded widths, and correlations of the joint spectrum and joint temporal intensity presented Fig. 2(a,d). All values are deconvolved to account for the finite resolution of the spectrometers and the temporal gate. Measured properties are widths in standard deviations and error bars are calculated from Monte Carlo simulations assuming Poissonian noise. A more comprehensive list including both raw and deconvolved fit parameters can be found in the Supplementary Material.

Property	Joint spectrum	Joint temporal intensity
Signal marginal width	$(10.56 \pm 0.04) \text{ ps}^{-1}$	$(0.537 \pm 0.009) \text{ ps}$
Signal heralded width	$(1.02 \pm 0.05) \text{ ps}^{-1}$	$(0.066 \pm 0.018) \text{ ps}$
Idler marginal width	$(9.69 \pm 0.03) \text{ ps}^{-1}$	$(0.587 \pm 0.015) \text{ ps}$
Idler heralded width	$(0.94 \pm 0.04) \text{ ps}^{-1}$	$(0.070 \pm 0.019) \text{ ps}$
Correlation ρ	-0.9951 ± 0.0001	0.987 ± 0.004

tral and temporal measurements are on the same order of magnitude as the spectral and temporal distributions, the measured features will be broadened. To account for this, the fit parameters are deconvolved assuming a Gaussian response function [40], and these values for the joint spectrum and joint temporal distribution of Fig. 2(a,d) are presented in Table I.

The measured joint spectrum shown in Fig. 2(a) exhibits strong anti-correlation (-0.9951 ± 0.0001) in the signal and idler frequencies, while the joint temporal intensity of Fig. 2(b) shows strong positive correlations (0.987 ± 0.004) in the arrival times of the photons. We can witness the effect of the spectral phase in Fig. 2(b,c), which show weak correlations between frequency of one photon and time of arrival of the other. Low correlations in the time-frequency plots may indicate little uncompensated dispersion in the experiment (see Supplementary Material).

The spectral and timing correlations are further analyzed by binning the data presented in Fig. 2(a,d) into histograms based on $\omega_1 + \omega_2$ and $t_s - t_i$, as well as $\omega_s - \omega_i$ and $t_s + t_i$ for comparison, as shown in Fig. 3. The bin size was selected to match the step size of the measurement apparatus. Gaussian fits to the histograms give a joint uncertainty product $\Delta(\omega_s + \omega_i)\Delta(t_s - t_i) = (1.429 \pm 0.006 \text{ ps}^{-1})(0.203 \pm 0.005 \text{ ps}) = 0.290 \pm 0.007$, which violates the inequality of Eq. 1 by about 100 standard deviations. Error bars are obtained via Monte-Carlo simulations assuming Poissonian noise. When deconvolved, we find $\Delta(\omega_s + \omega_i)\Delta(t_s - t_i) = (1.329 \pm 0.007 \text{ ps}^{-1})(0.110 \pm 0.010 \text{ ps}) = 0.15 \pm 0.01$. The measured uncertainty products thus provide a clear witness of energy-time entanglement on ultrafast timescales.

We now turn to the problem of measuring the impact of dispersion on our energy-time entangled state. We directly observe the effect of applied dispersion on the

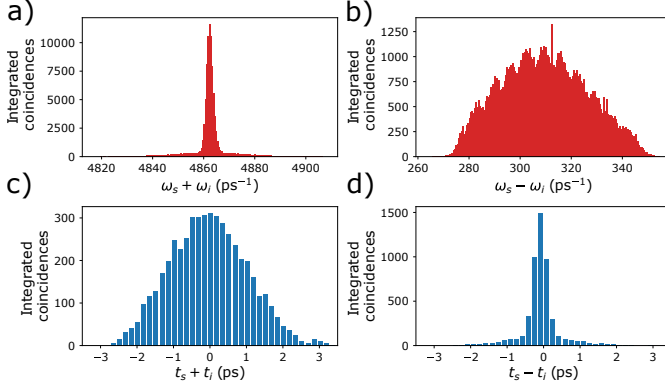


FIG. 3. **Histograms of the frequency and time of arrival correlations between signal and idler photons.** Coincidences are confined to a small region in (a) with $\Delta(\omega_s + \omega_i) = (1.429 \pm 0.006) \text{ ps}^{-1}$ ($1.329 \pm 0.007 \text{ ps}^{-1}$ when corrected for the finite resolution of the gate) compared to (b) with $\Delta(\omega_s - \omega_i) = (18.16 \pm 0.05) \text{ ps}^{-1}$ ($18.16 \pm 0.05 \text{ ps}^{-1}$) indicating strong anti-correlations in frequency. Likewise, coincidences are localized in (d) with $\Delta(t_s - t_i) = 0.203 \pm 0.005 \text{ ps}$ ($0.110 \pm 0.010 \text{ ps}$) compared to (c) with $\Delta(t_s + t_i) = 1.066 \pm 0.016 \text{ ps}$ ($1.052 \pm 0.016 \text{ ps}$) corresponding to strong correlations in the time of arrival. From these values, we find a joint uncertainty product $\Delta(\omega_s + \omega_i)\Delta(t_s - t_i) = 0.290 \pm 0.007$ (0.15 ± 0.01).

temporal correlations, as presented in the joint temporal intensities of Fig. 4. We control the spectral phase of the photons, $\phi(\omega_s, \omega_i) \approx A_s(\omega_s - \omega_{s0})^2 + A_i(\omega_i - \omega_{i0})^2$, with two grating compressors where the chirp parameters A_s and A_i are for the signal and idler fields, respectively. We estimate the magnitude of the applied dispersion from the geometry of the compressor and the relative position of the gratings [41], and measure the standard deviation $\Delta(t_s - t_i)$ of a Gaussian fit from histograms of $t_s - t_i$.

Starting from the case with no dispersion [Fig. 4(a)], we apply positive dispersion $A_s = (0.0373 \pm 0.0015) \text{ ps}^2$ to only the signal [Fig. 4(b)] and negative dispersion $A_i = -(0.0359 \pm 0.0014) \text{ ps}^2$ to only the idler [Fig. 4(c)]. In these two cases, we observe a large increase in the timing uncertainty $\Delta(t_s - t_i)$ and a vertical or horizontal shear of the joint-temporal intensity along the corresponding axis. We then apply the same amount of positive and negative dispersion to the signal and idler as before [Fig. 4(d)], where the dispersion applied to the idler is set to minimize the timing uncertainty between the two photons. Here, the timing uncertainty in arrival time $\Delta(t_s - t_i)$ is almost unchanged. This is the signature of nonlocal dispersion cancellation, limited by the finite correlations of the initial two-photon state (see Supplementary Material). The temporal marginals in Fig. 4(d) still increase since each side remains exposed to a significant amount of dispersion.

For classical pulses, the effect of dispersion on the correlations in arrival times can be expressed as an inequality [26], $\Delta(t_s - t_i)_F^2 \geq \Delta(t_s - t_i)_0^2 + 4A^2/\Delta(t_s - t_i)_0^2$,

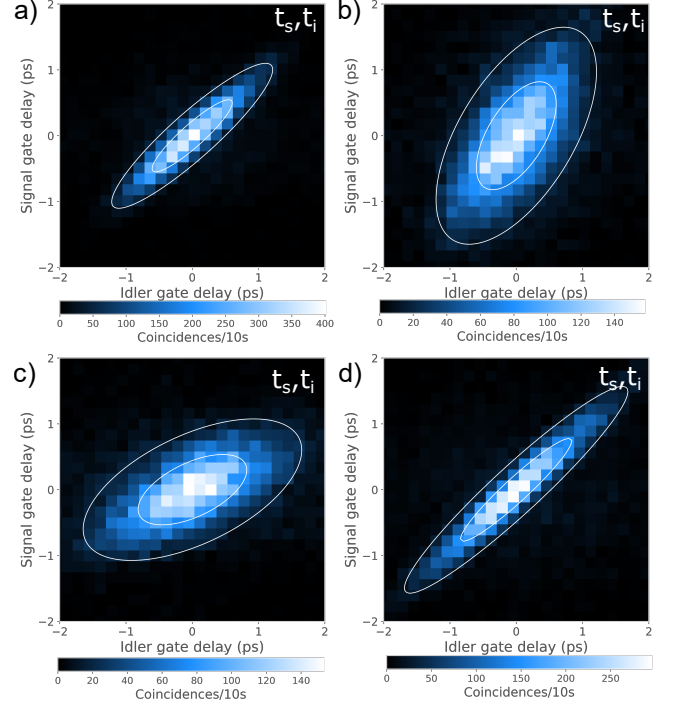


FIG. 4. **Nonlocal dispersion cancellation observed in the joint temporal distributions.** Joint temporal intensity for the signal and idler pair: (a) without dispersion, (b) with a positive dispersion of $A_s = (0.0373 \pm 0.0015) \text{ ps}^2$ on the signal, (c) with a negative dispersion of $A_i = (-0.0359 \pm 0.0014) \text{ ps}^2$ on the idler, and (d) with both a positive dispersion of $A_s = (0.0373 \pm 0.0015) \text{ ps}^2$ on the signal and a negative dispersion of $A_i = (-0.0359 \pm 0.0014) \text{ ps}^2$ on the idler. For each, we measure the uncertainty in the difference in arrival times of the signal and idler $\Delta(t_s - t_i)$ and find: (a) $0.235 \pm 0.003 \text{ ps}$ ($0.162 \pm 0.005 \text{ ps}$ when corrected for the finite resolution of the gate), (b) $0.708 \pm 0.013 \text{ ps}$ ($0.688 \pm 0.013 \text{ ps}$), (c) $0.714 \pm 0.010 \text{ ps}$ ($0.693 \pm 0.011 \text{ ps}$), (d) $0.245 \pm 0.004 \text{ ps}$ ($0.175 \pm 0.006 \text{ ps}$). We witness nonlocal dispersion cancellation in the timing uncertainty $t_s - t_i$ in (d) as the width $\Delta(t_s - t_i)$ remains almost unchanged with the one measured in (a).

where $\Delta(t_s - t_i)_0$ is the initial difference in detection times, and $\Delta(t_s - t_i)_F$ is the final difference with equal and opposite dispersion A applied on each side. Under the assumption that the initial state is unchirped, taking the measured initial value from Fig. 4(a), $\Delta(t_s - t_i)_0 = 0.235 \text{ ps}$ (0.162 ps when corrected for the gate resolution), and using the average magnitude of the applied dispersion $A = 0.0366 \text{ ps}^2$, we calculate that the standard deviation in arrival times for classical pulses has to be at least $\Delta(t_s - t_i)_F \geq 0.390 \text{ ps}$ (0.480 ps). However, the measured uncertainty observed in Fig. 4(d), $\Delta(t_s - t_i) = (0.245 \pm 0.004) \text{ ps}$, remains significantly smaller. The experimental apparatus thus provides a direct way to detect this inherently quantum effect in a regime inaccessible to current detectors.

We have directly measured both the temporal and frequency correlations of an ultrafast biphoton pulse. Optical gating employed here was critical for realizing ul-

trafast coincidence detection and correspondingly high-resolution temporal measurements. We observe energy-time entanglement via a joint time-bandwidth inequality and demonstrate ultrafast nonlocal dispersion cancellation of the biphotons with direct and independent detection. This work can be extended to quantum interference measurements on ultrafast timescales, and can be combined with temporal imaging to greatly increase the versatility of energy-time entangled photons for quantum information applications.

The authors thank M. Mazurek for fruitful discussions and M. Mastrovich for valuable assistance in the laboratory. This research was supported in part by the Natural Sciences and Engineering Research Council of Canada (NSERC), Canada Research Chairs, Industry Canada and the Canada Foundation for Innovation (CFI).

* jpmaclean@uwaterloo.ca

- [1] S. Ramelow, L. Ratschbacher, A. Fedrizzi, N. K. Langford, and A. Zeilinger, *Physical Review Letters* **103**, 253601 (2009).
- [2] I. Marcikic, H. de Riedmatten, W. Tittel, V. Scarani, H. Zbinden, and N. Gisin, *Physical Review A* **66**, 062308 (2002).
- [3] B. Brecht, D. V. Reddy, C. Silberhorn, and M. Raymer, *Physical Review X* **5**, 041017 (2015).
- [4] Q. Zhang, H. Takesue, S. W. Nam, C. Langrock, X. Xie, B. Baek, M. M. Fejer, and Y. Yamamoto, *Optics Express* **16**, 5776 (2008).
- [5] J. D. Franson, *Physical Review Letters* **62**, 2205 (1989).
- [6] J. D. Franson, *Physical Review A* **45**, 3126 (1992).
- [7] A. M. Steinberg, P. G. Kwiat, and R. Y. Chiao, *Physical review letters* **68**, 2421 (1992).
- [8] J. Nunn, L. J. Wright, C. Sller, L. Zhang, I. A. Walmsley, and B. J. Smith, *Optics Express* **21**, 15959 (2013).
- [9] J. M. Lukens, A. Dezfolyan, C. Langrock, M. M. Fejer, D. E. Leaird, and A. M. Weiner, *Physical Review Letters* **112**, 133602 (2014).
- [10] V. Giovannetti, S. Lloyd, and L. Maccone, *Nature* **412**, 417 (2001).
- [11] R. Trebino, K. W. DeLong, D. N. Fittinghoff, J. N. Sweetser, M. A. Krumbgel, B. A. Richman, and D. J. Kane, *Review of Scientific Instruments* **68**, 3277 (1997).
- [12] I. A. Walmsley and C. Dorrer, *Advances in Optics and Photonics* **1**, 308 (2009).
- [13] A. H. Zewail, *The Journal of Physical Chemistry A* **104**, 5660 (2000).
- [14] S.-W. Bahk, P. Rousseau, T. A. Planchon, V. Chvykov, G. Kalintchenko, A. Maksimchuk, G. A. Mourou, and V. Yanovsky, *Optics Letters* **29**, 2837 (2004).
- [15] Z. Chang, A. Rundquist, H. Wang, M. M. Murnane, and H. C. Kapteyn, *Physical Review Letters* **79**, 2967 (1997).
- [16] W. R. Zipfel, R. M. Williams, and W. W. Webb, *Nature Biotechnology* **21**, 1369 (2003).
- [17] S. Mancini, V. Giovannetti, D. Vitali, and P. Tombesi, *Physical Review Letters* **88**, 120401 (2002).
- [18] M. Avenhaus, A. Eckstein, P. J. Mosley, and C. Silberhorn, *Optics letters* **34**, 2873 (2009).
- [19] S. Schwarz, B. Bessire, and A. Stefanov, *International Journal of Quantum Information* **12**, 1560026 (2014).
- [20] O. Kuzucu, F. N. C. Wong, S. Kurimura, and S. Tovstonog, *Physical Review Letters* **101**, 153602 (2008).
- [21] L. K. Shalm, D. R. Hamel, Z. Yan, C. Simon, K. J. Resch, and T. Jennewein, *Nature Physics* **9**, 19 (2013).
- [22] Y.-W. Cho, K.-K. Park, J.-C. Lee, and Y.-H. Kim, *Physical Review Letters* **113**, 063602 (2014).
- [23] M. D. Eisaman, J. Fan, A. Migdall, and S. V. Polyakov, *Review of Scientific Instruments* **82**, 071101 (2011).
- [24] P. G. Kwiat, A. M. Steinberg, and R. Y. Chiao, *Physical Review A* **47**, R2472 (1993).
- [25] S. Agne, T. Kauten, J. Jin, E. Meyer-Scott, J. Z. Salvail, D. R. Hamel, K. J. Resch, G. Weihs, and T. Jennewein, *Physical Review Letters* **118**, 153602 (2017).
- [26] T. Wasak, P. Szakowski, W. Wasilewski, and K. Banaszek, *Physical Review A* **82**, 052120 (2010).
- [27] J. A. Jaramillo-Villegas, P. Imany, O. D. Odele, D. E. Leaird, Z.-Y. Ou, M. Qi, and A. M. Weiner, *Optica* **4**, 655 (2017).
- [28] S.-Y. Baek, Y.-W. Cho, and Y.-H. Kim, *Optics Express* **17**, 19241 (2009).
- [29] K. A. O'Donnell, *Physical Review Letters* **106**, 063601 (2011).
- [30] R. Prevedel, K. M. Schreier, J. Lavoie, and K. J. Resch, *Physical Review A* **84**, 051803 (2011).
- [31] O. Kuzucu, F. N. Wong, S. Kurimura, and S. Tovstonog, *Optics letters* **33**, 2257 (2008).
- [32] M. Allgaier, G. Vigh, V. Ansari, C. Eigner, V. Quiring, R. Ricken, Benjamin Brecht, and C. Silberhorn, *Quantum Science and Technology* **2**, 034012 (2017).
- [33] J. C. Howell, R. S. Bennink, S. J. Bentley, and R. W. Boyd, *Physical Review Letters* **92**, 210403 (2004).
- [34] M. Edgar, D. Tasca, F. Izdebski, R. Warburton, J. Leach, M. Agnew, G. Buller, R. Boyd, and M. Padgett, *Nature Communications* **3**, 984 (2012).
- [35] C. Chen, C. Bo, M. Y. Niu, F. Xu, Z. Zhang, J. H. Shapiro, and F. N. C. Wong, *Optics Express* **25**, 7300 (2017).
- [36] W. P. Grice and I. A. Walmsley, *Physical Review A* **56**, 1627 (1997).
- [37] W. P. Grice, A. B. U'Ren, and I. A. Walmsley, *Physical Review A* **64**, 063815 (2001).
- [38] A. Eckstein, A. Christ, P. J. Mosley, and C. Silberhorn, *Physical Review Letters* **106**, 013603 (2011).
- [39] G. Harder, V. Ansari, B. Brecht, T. Dirmeier, C. Marquardt, and C. Silberhorn, *Optics Express* **21**, 13975 (2013).
- [40] J. Donohue, M. Mastrovich, and K. Resch, *Physical Review Letters* **117**, 243602 (2016).
- [41] E. Treacy, *IEEE Journal of Quantum Electronics* **5**, 454 (1969).
- [42] R. Hanbury Brown and R. Q. Twiss, *Nature* **178**, 1046 (1956).
- [43] B. Brecht and C. Silberhorn, *Physical Review A* **87**, 053810 (2013).

SUPPLEMENTARY MATERIAL

Additional Experimental Details

The experiment uses a titanium-sapphire (Ti:Sapph) laser with an 80 MHz repetition rate which produces femtosecond laser pulses 12.5 ns apart centred at 775 nm with a $1/\sqrt{e}$ bandwidth of 2.25 nm. These are frequency doubled through second harmonic generation in 2 mm of type-I phasematched bismuth borate (BiBO) generating pulsed pump light centred at 387.5 nm with a $1/\sqrt{e}$ bandwidth of 0.6 nm and an average power of 900 mW. The resulting pump light is spectrally narrowed using a 0.085 nm ($1/\sqrt{e}$) bandpass filter, from which we estimate a pump coherence length of approximately 470 fs ($1/\sqrt{e}$). The remaining 300 mW of filtered pump is focussed in 5 mm of type-I BiBO for spontaneous parametric downconversion (SPDC). Signal-idler photon pairs are created with central wavelengths of 728.6 nm and 827.3 nm, respectively, and split with dichroic mirrors. These wavelengths are chosen such that the upconverted photon is spectrally far from the laser second-harmonic generation (SHG) background. The spectral bandwidths of the photons are controlled using a pair of short pass and long pass edge filters on each side. Each photon is then coupled into single-mode fibre and can be either be spectrally or temporally analyzed.

Spectral measurements are made with two grating-based scanning monochromators (1200 lines/mm), one for each of the two near-infrared (NIR) SPDC photons. See Ref. [40] for further details. The resolutions of the spectrometers, obtained from the emitted spectra of a Ne-Ar calibration lamp, are 0.081 nm and 0.135 nm for the signal and idler, respectively, the difference arising from slightly different slit widths in each monochromator.

For the temporal measurements, signal and idler photons are sent through 16.2 m and 21.2 m of fibre respectively. Grating-based compressors compensate for this chirp and allow variable control over the dispersion. A polarizing beam splitter separates the Ti:Sapph fundamental into two gates pulses. Due to the added propagation in fibre, the signal and idler photons originate respectively 7 and 9 pulses behind the gate pulses. Each photon then co-propagates with a gate pulse from the respective side with a spatial separation of about 8 mm and is subsequently focussed into 1 mm of type-I phasematched BiBO for sum-frequency generation (SFG). The upconverted light, with central wavelengths of 375 nm and 400 nm for the signal and idler sides, respectively, is recollimated, spectrally filtered with bandpass filters to remove second-harmonic background, and then coupled into multimode fibre. The SHG background was approximately 10 times higher for the idler SFG compared to the signal SFG and therefore, different gate powers were used to maximize the signal-to-noise ratios in each arm, with 500 mW for the signal gate pulse and 200 mW for the idler gate pulse. Both upconverted photons are detected with silicon avalanche photodiodes with quantum efficiencies of approximately 30% near 400nm. The coincidence window for detection events was set to 3 ns.

The relative separation of the gratings in each compressor is initially scanned to cancel the chirp from the fibres. This is achieved by minimizing the upconversion width as a function of the grating separation. The location of the minimum defines the centre position of the gratings in the compressor where zero dispersion is applied. The amount of dispersion provided by each compressor is then determined from the displacement of the gratings from their centre position and their angle with respect to the incident and reflected light. The compressors on the signal and idler arm are thus found to give 1315 fs^2 and 1925 fs^2 per mm of displacement, respectively, due to the inverse cubic dependence on wavelength [41].

Photons were produced at the source at a rate of 673,000 coincidence counts per second with 3.4×10^6 and 3.5×10^6 single-detection events per second for the signal and idler, respectively. The heralded second-order coherence of the source, measured with a Hanbury Brown-Twiss interferometer [42], was $g^{(2)}(0) = 0.416 \pm 0.004$ for the signal and $g^{(2)}(0) = 0.415 \pm 0.003$ for the idler. In general, double pair emission will lead to a broad background in the joint spectrum and joint temporal intensity. However, due to the tight temporal filtering on both sides, we estimate that double pairs contribute to less than 1% of the measured upconverted signal. After the upconversion on each side, approximately 30 coincidence counts (10,000 upconverted signal singles and 16,000 upconverted idler singles per second) per second were measured at the peak, from which about 0.6 coincidence counts (3,000 and 360 singles) per second were background from the second harmonic of the gate pulse.

See Table II for a list of parameters from the joint spectrum, joint temporal intensity, and frequency-time plots in Fig. 2 of the main text. See Table III for a collection of parameters for plots of the joint temporal intensity in Fig. 4. Raw measurements and deconvolved values are presented in both tables. The deconvolved width Δx is defined in terms of the measured width Δx_{meas} and the resolution of the instrument Δx_{res} . For example, for the marginals, we

TABLE II. **Complete fit parameters for joint plots.** Selected properties of the fits to the joint spectrum, joint temporal intensity, and joint time frequency plots seen in Fig. 2 of the main text. Values in parentheses are deconvolved from a Gaussian response function.

Property (Deconvolved)		Joint-spectrum	Joint-temporal intensity	Signal frequency Idler time	Signal time Idler frequency
Signal	Frequency (ω)	$2586.9 \pm 0.4 \text{ ps}^{-1}$	-	-	-
	Marginal width	$10.57 \pm 0.04 \text{ ps}^{-1}$ ($10.56 \pm 0.04 \text{ ps}^{-1}$)	$0.550 \pm 0.009 \text{ ps}$ ($0.537 \pm 0.009 \text{ ps}$)	$9.43 \pm 0.05 \text{ ps}^{-1}$ ($9.42 \pm 0.05 \text{ ps}^{-1}$)	$0.533 \pm 0.003 \text{ ps}$ ($0.519 \pm 0.003 \text{ ps}$)
	Heralded width	$1.16 \pm 0.04 \text{ ps}^{-1}$ ($1.02 \pm 0.05 \text{ ps}^{-1}$)	$0.176 \pm 0.008 \text{ ps}$ ($0.066 \pm 0.018 \text{ ps}$)	$9.4 \pm 0.2 \text{ ps}^{-1}$ ($9.3 \pm 0.2 \text{ ps}^{-1}$)	$0.514 \pm 0.017 \text{ ps}$ ($0.501 \pm 0.018 \text{ ps}$)
Idler	Frequency (ω)	$2276.9 \pm 0.3 \text{ ps}^{-1}$	-	-	-
	Marginal width	$9.69 \pm 0.03 \text{ ps}^{-1}$ ($9.69 \pm 0.03 \text{ ps}^{-1}$)	$0.600 \pm 0.015 \text{ ps}$ ($0.587 \pm 0.015 \text{ ps}$)	$0.589 \pm 0.006 \text{ ps}$ ($0.576 \pm 0.006 \text{ ps}$)	$8.03 \pm 0.05 \text{ ps}^{-1}$ ($8.02 \pm 0.05 \text{ ps}^{-1}$)
	Heralded width	$1.06 \pm 0.04 \text{ ps}^{-1}$ ($0.94 \pm 0.04 \text{ ps}^{-1}$)	$0.185 \pm 0.009 \text{ ps}$ ($0.070 \pm 0.019 \text{ ps}$)	$0.588 \pm 0.022 \text{ ps}$ ($0.576 \pm 0.022 \text{ ps}$)	$7.7 \pm 0.6 \text{ ps}^{-1}$ ($7.7 \pm 0.6 \text{ ps}^{-1}$)
Statistical Correlation		-0.9939 ± 0.0001 (-0.9951 ± 0.0001)	0.944 ± 0.003 (0.987 ± 0.004)	0.109 ± 0.008 (0.111 ± 0.008)	-0.103 ± 0.008 (-0.106 ± 0.008)

TABLE III. **Complete fit parameters for the nonlocal dispersion cancellation.** Selected properties of the fits to the joint temporal intensity plots seen in Fig. 4 of the main text. Values in parentheses are deconvolved from a Gaussian response function.

Property (Deconvolved)		No dispersion	Positive dispersion on the signal	Negative dispersion on the idler	Opposite dispersion
Signal	Marginal width	$0.536 \pm 0.004 \text{ ps}$ ($0.523 \pm 0.004 \text{ ps}$)	$0.797 \pm 0.009 \text{ ps}$ ($0.788 \pm 0.009 \text{ ps}$)	$0.518 \pm 0.004 \text{ ps}$ ($0.504 \pm 0.004 \text{ ps}$)	$0.764 \pm 0.007 \text{ ps}$ ($0.754 \pm 0.007 \text{ ps}$)
	Heralded width	$0.206 \pm 0.010 \text{ ps}$ ($0.132 \pm 0.012 \text{ ps}$)	$0.619 \pm 0.040 \text{ ps}$ ($0.599 \pm 0.040 \text{ ps}$)	$0.405 \pm 0.020 \text{ ps}$ ($0.384 \pm 0.021 \text{ ps}$)	$0.230 \pm 0.030 \text{ ps}$ ($0.160 \pm 0.030 \text{ ps}$)
Idler	Marginal width	$0.592 \pm 0.006 \text{ ps}$ ($0.580 \pm 0.006 \text{ ps}$)	$0.585 \pm 0.005 \text{ ps}$ ($0.572 \pm 0.005 \text{ ps}$)	$0.795 \pm 0.010 \text{ ps}$ ($0.786 \pm 0.010 \text{ ps}$)	$0.820 \pm 0.010 \text{ ps}$ ($0.811 \pm 0.010 \text{ ps}$)
	Heralded width	$0.223 \pm 0.012 \text{ ps}$ ($0.143 \pm 0.014 \text{ ps}$)	$0.448 \pm 0.013 \text{ ps}$ ($0.428 \pm 0.014 \text{ ps}$)	$0.613 \pm 0.004 \text{ ps}$ ($0.592 \pm 0.004 \text{ ps}$)	$0.231 \pm 0.015 \text{ ps}$ ($0.160 \pm 0.020 \text{ ps}$)
Statistical Correlation		0.912 ± 0.003 (0.956 ± 0.003)	0.589 ± 0.009 (0.609 ± 0.009)	0.56 ± 0.01 (0.58 ± 0.01)	0.951 ± 0.002 (0.973 ± 0.002)

have $\Delta x = \sqrt{\Delta x_{\text{meas}}^2 - \Delta x_{\text{res}}^2}$.

Signatures of energy-time entanglement

In this section, we calculate the joint-uncertainty product $\Delta(\omega_s + \omega_i)\Delta(t_s - t_i)$ using a model for a two-photon state with variable energy-time entanglement [30, 40]. We show that entangled quantum states can violate the inequality of Eq. 1 and describe the time-bandwidth products (TBP) of this state. This requires calculating both the joint spectral intensity and the joint temporal intensity.

Consider the correlated two-mode state,

$$|\psi\rangle = \int d\omega_s d\omega_i F(\omega_s, \omega_i) a_{\omega_s}^\dagger a_{\omega_i}^\dagger |0\rangle, \quad (2)$$

with the normalized joint-spectral amplitude expressed in Gaussian form as,

$$F(\omega_s, \omega_i) = \frac{1}{\sqrt{2\pi\sigma_{\omega_s}\sigma_{\omega_i}}(1-\rho_\omega^2)^{1/4}} \exp\left(-\frac{1}{2(1-\rho_\omega^2)} \left[\frac{(\omega_s - \omega_{s0})^2}{2\sigma_{\omega_s}^2} + \frac{(\omega_i - \omega_{i0})^2}{2\sigma_{\omega_i}^2} - \frac{\rho_\omega(\omega_s - \omega_{s0})(\omega_i - \omega_{i0})}{\sigma_{\omega_s}\sigma_{\omega_i}} \right]\right). \quad (3)$$

In the two-mode state of Eq. 3, there are two relevant length scales for the signal and idler, which we refer to as the marginal width, $\Delta\omega^{(m)}$, and the heralded or coincident width, $\Delta\omega^{(h)}$, and where, here, $\Delta x = \sqrt{\langle x^2 \rangle - \langle x \rangle^2}$ refers to the intensity standard deviation or $1/\sqrt{e}$ width of the variable x . The marginal widths in the equation are obtained by taking the marginal over one photon and tracing out or ignoring the other, while the heralded widths are obtained by fixing the frequency of either the signal or idler to its central frequency ($\omega_s \rightarrow \omega_{s0}$ or $\omega_i \rightarrow \omega_{i0}$). Using Eq. 3 above, we find,

$$\Delta\omega_{s,i}^{(m)} = \sigma_{\omega_{s,i}} \quad (4)$$

$$\Delta\omega_{s,i}^{(h)} = \sqrt{1 - \rho_\omega^2} \sigma_{\omega_{s,i}} \quad (5)$$

The correlation parameter $\rho_\omega = \Delta(\omega_s\omega_i)/\Delta\omega_s\Delta\omega_i$ describes the statistical correlations between the frequency of the signal and idler modes and is related to the purity of the partial trace, $P = \sqrt{1 - \rho_\omega^2}$. When $\rho_\omega = 0$, the joint-spectral amplitude $F(\omega_s, \omega_i)$ factorizes and the state is separable, whereas when $\rho_\omega \rightarrow -1$, the photons are perfectly anti-correlated in frequency and when $\rho_\omega \rightarrow 1$, they are perfectly correlated.

The joint temporal amplitude is obtained by taking the Fourier transform of the joint spectral amplitude,

$$\begin{aligned} f(t_s, t_i) &= \int d\omega_i d\omega_s F(\omega_i, \omega_s) e^{i\omega_i t_i} e^{i\omega_s t_s} \\ &= \frac{1}{\pi} \sqrt{2\pi\sigma_{\omega_s}\sigma_{\omega_i}} (1 - \rho_\omega^2)^{1/4} \exp\left(-t_s^2\sigma_{\omega_s}^2 - t_i^2\sigma_{\omega_i}^2 - 2t_s t_i \rho_\omega \sigma_{\omega_s} \sigma_{\omega_i} - i(t_s \omega_{s0} + t_i \omega_{i0})\right). \end{aligned} \quad (6)$$

Equation 6 can be recast as a two-dimensional Gaussian in the form of Eq. 3 and in doing so, we obtain expressions for the marginal pulse width $\Delta t^{(m)}$ and the heralded pulse width $\Delta t^{(h)}$ for the signal and idler, as well as the statistical correlations ρ_t between the time of arrival of the photons,

$$\Delta t_{s,i}^{(m)} = \frac{1}{2\sqrt{1 - \rho_\omega^2} \sigma_{\omega_{s,i}}} \quad (7)$$

$$\Delta t_{s,i}^{(h)} = \frac{1}{2\sigma_{\omega_{s,i}}} \quad (8)$$

$$\rho_t = -\rho_\omega. \quad (9)$$

We observe that the marginal pulse width $\Delta t^{(m)}$ is inversely proportional to the heralded bandwidth $\sqrt{1 - \rho_\omega^2} \sigma_\omega$ and heralded pulse widths $\Delta t^{(h)}$ is inversely proportional to the marginal bandwidth σ_ω . In addition, the statistical correlations in the temporal intensity, ρ_t , are reversed from those in the spectral intensity, ρ_ω .

Joint-uncertainty product

Using both joint amplitude functions of Eq. 3 and Eq. 6, we can calculate the variance in the sum of the frequencies of the signal and idler,

$$\Delta(\omega_s + \omega_i)^2 = \sigma_{\omega_s}^2 + 2\rho_\omega \sigma_{\omega_i} \sigma_{\omega_s} + \sigma_{\omega_i}^2, \quad (10)$$

and variance in the difference in time of arrival,

$$\Delta(t_s - t_i)^2 = \frac{\sigma_{\omega_s}^2 + 2\rho_\omega \sigma_{\omega_i} \sigma_{\omega_s} + \sigma_{\omega_i}^2}{4(1 - \rho_\omega^2) \sigma_{\omega_i}^2 \sigma_{\omega_s}^2}, \quad (11)$$

in order to obtain the joint uncertainty product,

$$\Delta(\omega_s + \omega_i) \Delta(t_s - t_i) = \sqrt{\frac{(\sigma_{\omega_s}^2 + 2\rho_\omega \sigma_{\omega_i} \sigma_{\omega_s} + \sigma_{\omega_i}^2)^2}{4(1 - \rho_\omega^2) \sigma_{\omega_i}^2 \sigma_{\omega_s}^2}}. \quad (12)$$

If the bandwidths $\sigma_{\omega_s} = \sigma_{\omega_i}$ are equal, then for the state above, the joint uncertainty product is $\Delta(\omega_s + \omega_i) \Delta(t_s - t_i) = \sqrt{(1 + \rho_\omega)/(1 - \rho_\omega)}$. In this case, the joint uncertainty product for the transform limited two-photon state depends entirely on the frequency correlation parameter ρ_ω . When $\rho_\omega < 0$, the state clearly violates Eq. 1; the simultaneous correlations in frequency and time are stronger than those achievable with classical pulses and the state is energy-time entangled. When $\rho_\omega = 0$, the state satisfies the equality as it is separable. The presence of dispersion on either photon increases the overall product. Spectral phase stretches the temporal profile of the photons and increases the uncertainty $\Delta(t_s - t_i)$ in their arrival time without affecting the uncertainty in the bandwidth $\Delta(\omega_s + \omega_i)$. If the photons are positively correlated $\rho_\omega > 0$, a different joint-uncertainty product can be used to verify entanglement, namely $\Delta(\omega_s - \omega_i) \Delta(t_s + t_i)$ which is also always greater than or equal to one for separable states.

Time-bandwidth products

From the joint spectral and joint temporal amplitude functions, we can also obtain a set of time-bandwidth products (TBP) for the individual modes. For a classical pulse, the TBP must satisfy the uncertainty relation,

$$\Delta\omega \Delta t \geq 1/2. \quad (13)$$

On the other hand, for correlated photons, there are four possible time-bandwidth products. The first two time-bandwidth products of the individual photons compare the marginal (heralded) bandwidth to the heralded (marginal) temporal pulse width. For the Fourier limited two-photon state presented above, using Eqs. 4, 5, 7, and 8, they are,

$$\Delta\omega^{(m)} \Delta t^{(h)} = 1/2 \quad (14)$$

$$\Delta\omega^{(h)} \Delta t^{(m)} = 1/2. \quad (15)$$

These TBPs take place of the classical time-bandwidth products, and hold regardless of the amount of entanglement in the system. In the presence of a nonzero spectral phase, the temporal widths will increase whereas the frequency widths will remain the same, and the TBP will only get larger. The value 1/2 is thus a minimum which is attained when there is no spectral phase.

The last two TBPs compare both marginal widths and both heralded widths, and we find,

$$\Delta\omega^{(m)} \Delta t^{(m)} = \frac{1}{2} \frac{1}{\sqrt{1 - \rho_\omega^2}} \quad (16)$$

$$\Delta\omega^{(h)} \Delta t^{(h)} = \frac{1}{2} \sqrt{1 - \rho_\omega^2}. \quad (17)$$

These TBPs depend on the strength of the frequency correlations ρ_ω . Both reduce to 1/2 when there are no correlation and the state is spectrally pure, $\rho_\omega = 0$. The marginal TBP, $\Delta\omega^{(m)} \Delta t^{(m)}$, will increase for a correlated state $0 < |\rho_\omega| < 1$, whereas the heralded TBP, $\Delta\omega^{(h)} \Delta t^{(h)}$, will decrease. Energy-time entangled states can have a heralded TBP much smaller than 1/2 when $\rho_\omega < 0$. Since this is forbidden for classical pulses, it can also be used as a measure of entanglement, and has been shown to be directly related to the spectral purity of the state [43]. Similarly to the two previous TBPs, both the marginal TBP and the heralded TBP will increase in the presence of nonzero spectral phase.

Energy-time entanglement with dispersion

We next analyze the effect of dispersion on the energy-time entangled state in order to determine its effect on the joint-uncertainty product and the conditions under which nonlocal dispersion cancellation can be observed. Starting with the joint spectral amplitude in Eq. 3, we apply dispersion to both photons,

$$F(\omega_s, \omega_i) \rightarrow F(\omega_s, \omega_i) e^{i\phi(\omega_s, \omega_i)}, \quad (18)$$

and assume spectral phase has the separable form, $\phi(\omega_s, \omega_i) = A_i(\omega_i - \omega_{i0})^2 + A_s(\omega_s - \omega_{s0})^2$, with chirp parameters A_i and A_s . The presence of spectral phase will not affect any of the spectral intensity measurements. It will, however, stretch the temporal marginal of the photons, and we can witness this change in the increase of the marginal pulse widths,

$$\Delta t_{s,i}^{(m)} = \sqrt{\frac{1}{4(1 - \rho_\omega^2)\sigma_{s,i}^2} + 4A_{s,i}^2\sigma_{\omega_{s,i}}^2}. \quad (19)$$

The marginal width in time with dispersion has two terms. The first term is the Fourier limited marginal width found in Eq. 7. When the chirp parameter is nonzero, $A_{s,i} \neq 0$, for the signal or the idler, we see an increase in the corresponding marginal due to the second term $4A_{s,i}^2\sigma_{s,i}^2$, regardless of the sign of $A_{s,i}$. Moreover, the dispersion A is applied to the entire marginal frequency bandwidth σ_ω . On the other hand, the joint temporal properties of the photons do depend on the relative sign of A_i and A_s , and we can observe this in the heralded pulse width $\Delta t_s^{(h)}$ or in the variance of the difference in time of arrival of the signal and idler $\Delta(t_s - t_i)^2$. For example, the signal heralded pulse width under dispersion is,

$$\Delta t_s^{(h)} = \sqrt{\frac{1}{4\sigma_s^2} + 4A_s^2(1 - \rho_\omega^2)\sigma_s^2 + \frac{4\rho_\omega^2(A_s\sigma_s^2 + A_i\sigma_i^2)^2}{\sigma_s^2(1 + 16A_i^2(1 - \rho^2)\sigma_i^4)}}, \quad (20)$$

the idler heralded pulse width $\Delta t_i^{(h)}$ is obtained from Eq. 20 by exchanging all subscripts s with subscripts i , and the variance $\Delta(t_s - t_i)^2$ is,

$$\Delta(t_s - t_i)^2 = \frac{\sigma_s^2 + 2\rho_\omega\sigma_i\sigma_s + \sigma_i^2}{4(1 - \rho_\omega^2)\sigma_i^2\sigma_s^2} + 4(A_s\sigma_s + A_i\sigma_i)^2 - 8A_iA_s(1 + \rho_\omega)\sigma_i\sigma_s. \quad (21)$$

We focus on the variance, $\Delta(t_s - t_i)^2$, in Eq. 21 as the other two heralded pulse widths have a similar structure. We find that it consists of three distinct terms: the first is the Fourier-limited variance when no chirp is applied as in Eq. 11, the second is the origin of the nonlocal dispersion cancellation as it goes to 0 when $A_s\sigma_s = -A_i\sigma_i$, and the third results from the finite correlations in the model and also goes to zero for perfect anti-correlations $\rho_\omega \rightarrow -1$. The variance in Eq. 21 can only increase in the presence of dispersion, and therefore, the same holds for the joint-uncertainty product of Eq. 1.

In order to observe complete nonlocal dispersion cancellation for frequency anti-correlated photons, two conditions must be met: the dispersion must be opposite in sign with ratios given by $A_s\sigma_s = -A_i\sigma_i$, and the photons must be perfectly anti-correlated in frequency, $\rho_\omega = -1$. In the present experiment, the first condition is satisfied by setting the signal chirp A_s and finding the idler chirp A_i that minimizes the uncertainty in arrival time. However, since we apply dispersion to photons with finite correlations, $\rho_\omega > -1$, the second condition isn't met exactly, and this contributes to increasing the spread in arrival times $\Delta(t_s - t_i)$ as observed in the imperfect cancellation of Fig. 4(d).

Measurements of frequency-time correlations as an indication of dispersion

We now illustrate how the measurements of the cross-correlation in the frequency of one photon and time of arrival of the other provide information on the dispersion. A temporal measurement is applied to the signal photon ω_s and a spectral measurement is applied to the idler photon ω_i . The temporal measurement is modelled as a convolution of the input signal photon spectra with the gate pulse,

$$G(\omega_g, \tau) = \frac{1}{(2\pi\sigma_g^2)^{\frac{1}{4}}} \exp\left(-\frac{(\omega_g - \omega_{g0})^2}{4\sigma_g^2} + i\tau(\omega_g - \omega_{g0})\right) \quad (22)$$

which has centre frequency ω_g , marginal bandwidth σ_g , and delay τ . The upconverted photon at frequency $\omega_3 = \omega_s + \omega_g$, is then measured in coincidence with the spectrally filtered idler photon ω_2 , and the probability of measuring a coincidence is,

$$S(\tau_s, \omega_i) = \int d\omega_3 | \int d\omega_s G(\omega_3 - \omega_s, \tau_s) \Phi_{\text{SFG}}(\omega_s, \omega_3 - \omega_s, \omega_3) F(\omega_s, \omega_i) |^2, \quad (23)$$

where Φ_{SFG} is the phasematching function of the sum-frequency generation process in the temporal measurement and $F(\omega_s, \omega_i)$ is the joint spectral amplitude. For simplicity, we assume the phasematching is infinitely broad $\Phi_{\text{SFG}} \approx 1$. While this assumption isn't strictly valid, the phasematching for the crystals used in the experiment isn't strong enough to change the intuition presented here.

Since the convolution of two Gaussians is a Gaussian, we can re-express $S(\tau_s, \omega_i)$ of Eq. 23 as a two-dimensional Gaussian such as in Eq. 3, with the marginal bandwidth $\Delta\omega_i^{(m)}$, marginal pulse width $\Delta t_s^{(m)}$, and statistical correlation ρ_f as follows,

$$\Delta\omega_i^{(m)} = \sigma_s \quad (24)$$

$$\Delta t_s^{(m)} = \sqrt{\frac{1}{4\sigma_g^2} + \frac{1}{4(1-\rho_\omega^2)\sigma_s^2} + 4A_s^2\sigma_s^2} \quad (25)$$

$$\rho_f = \frac{-4A_s\rho_\omega\sqrt{1-\rho_\omega^2}\sigma_g\sigma_s^2}{\sqrt{(1-\rho_\omega^2)\sigma_s^2 + \sigma_g^2(1+16A_s^2(1-\rho_\omega^2)\sigma_s^4)}}. \quad (26)$$

We see that the marginal bandwidth of the idler $\Delta\omega_i^{(m)}$ in Eq. 24 is independent to the chirp A_i as the spectral measurement is independent of phase. In the limit of zero chirp on the signal, $A_s = 0$, the marginal pulse width $\Delta t_s^{(m)}$ in Eq. 25 is a quadrature sum of the gate pulse width $1/2\sigma_g$ and the coherence length of the signal $1/(2\sqrt{1-\rho_\omega^2}\sigma_s)$ from Eq. 7, and the frequency of the idler and time of arrival of the signal are uncorrelated, $\rho_f = 0$ in Eq. 26. When $A_s \neq 0$, the signal marginal is stretched by the presence of the extra term $4A_s^2\sigma_s^4$ in Eq. 25, the same term that appears in Eq. 19, and the correlations increase with $-A_s$ in Eq. 26.

The effect of phase-matching is now briefly considered. Second-order phasematching effects describes photons of different frequencies walking off from each other inside the crystal. In the SFG process considered here, a photon and gate pulse in the NIR are upconverted to produce a higher energy photon in the ultraviolet. When the upconverted photon walks off from the signal and gate, the upconversion becomes partially mode selective and is no longer sensitive to all frequencies[3]. Since the photons are correlated in frequency, the effective frequency filtering on one side has the effect of reducing the measured spectral bandwidth of the photon on the other side. We observe this slight reduction when comparing the marginal bandwidth in the joint spectrum and frequency-time plots in Table II.

Additional Experimental Results

Time-bandwidth products

The four additional measured TBPs are presented in Table IV. We find that the first two TBPs approach the value of 1/2 obtained for a Fourier limited two-dimensional Gaussian pulse. The difference between the measured values and the value of 1/2 could be due to a few reasons. Uncompensated dispersion will increase both TBPs. The time-frequency plots do exhibit small correlations in Fig. 2, which would also arise from a nonzero spectral phase. In addition, bandwidth filtering will increase the heralded width $\Delta t^{(h)}$ as it depends directly on the marginal spectrum and thus further increase $\Delta\omega^{(m)}\Delta t^{(h)}$. We observe a small amount of spectral clipping from the edge filters in the source which will reduce the spectral bandwidth of the photons. Any bandwidth filtering from the grating compressors would have the same effect. Moreover, since the heralded width depends on the measurements on both the signal and idler side, errors associated with it tend to be larger. This error translates to the deconvolved value, and the measured error on the TBPs involving $\Delta t^{(h)}$.

When observing the other two TBPs, we find that the marginal TBP $\Delta\omega^{(m)}\Delta t^{(m)}$ is much larger than the minimum of 1/2. This is consistent with either a mixed state or a spectrally correlated state. The heralded TBP $\Delta\omega^{(h)}\Delta t^{(h)}$ is smaller than the classically allowed value of 1/2, providing yet another confirmation that the photons exhibit energy-time entanglement.

TABLE IV. **Time-bandwidth products.** The four time-bandwidth products of the signal and idler photons from SPDC are obtained from the marginal and heralded widths of Fig. 2(a,d). Values in parentheses are deconvolved with a Gaussian response function.

TBP (Deconvolved)	Signal	Idler
$\Delta\omega^{(m)}\Delta t^{(h)}$	1.64 ± 0.07 (0.62 ± 0.15)	1.64 ± 0.09 (0.62 ± 0.16)
$\Delta\omega^{(h)}\Delta t^{(m)}$	0.63 ± 0.03 (0.55 ± 0.03)	0.64 ± 0.03 (0.55 ± 0.03)
$\Delta\omega^{(m)}\Delta t^{(m)}$	5.16 ± 0.07 (5.03 ± 0.07)	5.3 ± 0.1 (5.2 ± 0.1)
$\Delta\omega^{(h)}\Delta t^{(h)}$	0.20 ± 0.01 (0.07 ± 0.02)	0.20 ± 0.01 (0.07 ± 0.02)